JOURNAL OF THE SOUTHEASTERN ASSOCIATION FOR RESEARCH IN ASTRONOMY, **2**, 64-70, 2008 MAY 1

INITIAL MEASUREMENT OF INTRAPIXEL VARIATIONS IN BACK-ILLUMINATED, HIGH-RESISTIVITY, P-CHANNEL, CHARGE COUPLED DEVICES

JASON PULS[1]
Physics Department 118 Kinard Laboratory, Clemson University, Clemson, SC 29634-0978

HAKEEM M. OLUSEYI
Department of Physics and Space Sciences, Florida Institute of Technology, Melbourne, FL 32901

ABSTRACT

In 1929 Edwin Hubble discovered the universe's expansion. Seventy years later it was unexpectedly found that the rate of expansion is accelerating due to some vast cosmic energy. This cosmic energy, apparently gravitationally repulsive and spread homogeneously through the universe, has come to be known as dark energy. To better understand this universal force, scientists utilize Type Ia supernovae and weak gravitational lensing as cosmological probes. Lawrence Berkeley National Laboratory (LBNL) is developing the Supernova Acceleration Probe (SNAP), a proposed space-based telescope that will be used to identify and measure supernovae and measure weak gravitational lensing signals across fifteen square degrees of the sky. The SNAP telescope will incorporate an innovative camera that consists of back-illuminated, high-resistivity, p-channel charged coupled devices (CCDs) for visible to near-infrared light detection. Presented are results obtained from the measurement and analysis of a 10.5 μm pixel pitch, 1.4k by 1.4k format, p-channel CCD fabricated on high-resistivity silicon at LBNL. The fully depleted device is 300 μm thick and backside illuminated. We report on the first measurement of the intrapixel sensitivity and spatial variations of these CCDs. We also report measurements of electric field distortions near the edges of the CCD active area.

Subject headings: charge coupled devices, CCDs, Supernova Acceleration Probe, SNAP, dark energy, dark matter, cosmology

1. INTRODUCTION

In the early 1900s Edwin Hubble used what was, at the time, the largest telescope in the world to study cepheid variables. He developed a law, known as Hubble's Law, that formed a relationship between galactic redshifts and distances (Hubble 1929) thus discovering the universal expansion. Subsequently it was expected that the universe's expansion was decelerating due to the gravitation of matter within it. Teams of astronomers spent years trying to find the rate of the deceleration but to no avail. In 1998 the astrophysics community was stunned with the discovery that the universe was accelerating (Riess et al. 1998; Perlmutter et al. 1999). It seemed that some invisible energy, now coined "dark energy," was pushing the universe apart. Because of its effect on the universe and its mysterious relationship with our current views of physical laws, dark energy is one of the most important topics of modern scientific research.

1.1. *Measuring Dark Energy*

There are two techniques for studying the expansion rate of the universe that are both relatively mature and possess acceptable measurement errors. One of these is by using Type Ia supernovae (SNe Ia) as standard candles. These types of supernovae occur when a white dwarf star slowly accretes matter from its companion in a binary system. When the dwarf approaches the Chandresakhar Limit it explodes. These are viable standard candles because the masses of the SNe Ia upon exploding are all very nearly the same. They are also easy to distinguish due to the strong silicon absorption observable in their spectral lines. By comparing the apparent magnitude of the SN Ia to its calibrated intrinsic magnitude, its distance can be calculated. Because the speed of light is a known value, the time since the light was sent from the SN Ia can also be determined. We also know that as the universe expands, the light that is moving through it becomes stretched by exactly the same amount. Thus by looking at the spectrum of the incoming light, the expansion of the universe during the light's travel can also be seen. Using these SNe Ia, the universe's expansion rate can be found with respect to time.

The other technique for studying the expansion of the universe is by mapping the contents and dynamics of the universe. This can be accomplished using a technique called gravitational weak lensing. When the background universe is imaged, differences in the uniformity of foreground matter can cause warping to be seen. The statistical patterns seen in the warping are in a direct relationship to the matter concentrations along the line of sight. If one obtains a measurement of the redshift of both the foreground matter and the background matter, one can combine this information with the distortions to calculate the number and sizes of matter concentrations as a function of distance (and hence time) along the line of sight. This measurement thus allows one to measure the growth rate of matter concentrations along the line of sight. Since gravity pulls galaxies together and dark energy pushes them apart, measurement of the growth of structures in the universe provides information about dark energy.

1.2. *The* Supernova Acceleration Probe

These two techniques, utilizing SN Ia and weak gravitational lensing, require an advanced, space-based instrument. The Lawrence Berkeley National Laboratory (LBNL) is in the process of developing this powerful new observatory, the

[1] Southeastern Association for Research in Astronomy (SARA) NSF-REU Summer Intern
Electronic address: jpuls@clemson.edu; holuseyi@fi t.edu

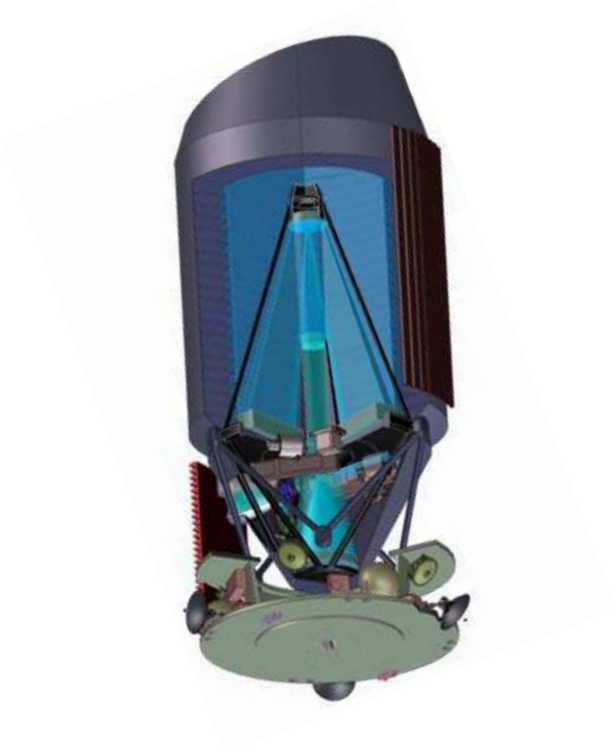

FIG. 1.— The SNAP satellite. (courtesy LBNL)

Supernova Acceleration Probe satellite (SNAP) (Aldering et al. 2002, 2004). SNAP is a 2-meter, space-based telescope (Fig. 1) scheduled to launch in 2013. SNAP will undertake measurements of SN Ia light curves and spectra, and will also generate gravitational weak lensing maps over large regions of the sky. Performing these measurements at the required accuracy, precision, and stability in the harsh environs of space places strict requirements on SNAP detector technologies.

SNAP's imager camera (Fig. 2) will be integrated with two imaging sensor systems: the LBNL high-resistivity, p-channel charged coupled devices (CCDs) for the visible (Holland et al. 1996, 1997) (Fig.3) and HgCdTe sensors for the near infrared. High-resisitivity, p-channel CCDs offer several advantages over other types. These include sensitivity to a wider range of light energies and wavelengths (Stover et al. 1997; Holland et al. 2003; Oluseyi et al. 2004, 2005), improved radiation tolerance (Bebek et al. 2002; Marshall et al. 2004; Dawson et al. 2006) (an important factor for the longevity of precision measurements with SNAP), and improved control over spatial information (Karcher et al. 2003; Fairfield et al. 2006).

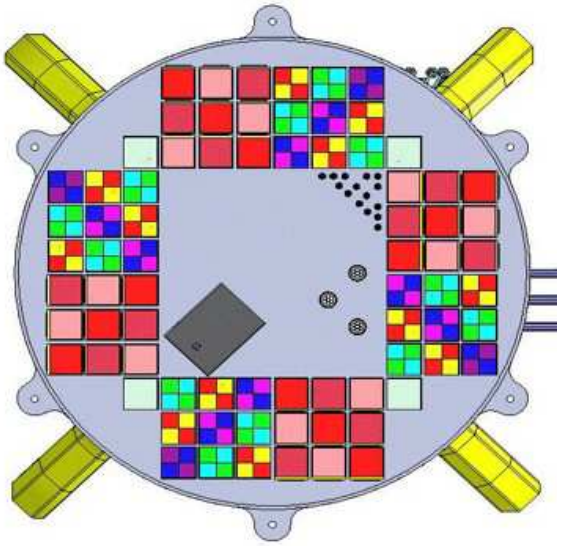

FIG. 2.— The SNAP focal plane incorporates 36 3.5k x 3.5k 10.5um high-resistivity, p-channel CCDs with four color filters on each and 36 HgCdTe near infrared devices. (courtesy LBNL)

For SNAP to achieve its science goals it is necessary to make measurements of the absolute magnitudes of SNe Ia and the shapes of galaxies with both high precision and high fidelity (Aldering et al. 2004). Light creates a bundle of charges near the CCD's backside, which spread due to diffusion prior to being collected in the frontside CCD circuitry. In order to perform weak lensing science, it is necessary to characterize and control the amount of spreading caused by diffusion. Moreover, simulations suggest that near the device edges electric fields become distorted (Fig. 4). This distortion would tend to modify the shapes of any galaxy images falling on these regions of the device. The accuracy and precision of photometric measurements may be limited by pixel to pixel and intrapixel response variations negatively affecting SNAP's ability to acquire accurate SN Ia light curves and the photometric redshift measurements of foreground and background matter concentrations necessary for performing weak lensing science.

Our work here is focused on measuring the intrapixel variations of the CCDs. This report describes analysis of data taken on backside illuminated, high-resisitivity, p-channel CCDs similar to the type that will be used on SNAP. This data was analyzed to look into the intrapixel variations of the CCD and to observe pixels near the edge of the device to determine their accuracy. These results may prove to be very important to the success of the SNAP telescope.

2. DATA ACQUISITION

The data used in the analysis was obtained from a 10.5 μm pixel pitch, 1.4k $\times$ 1.4k format, 300 μm thick, p-channel CCD that was operated fully depleted via a 40V bias voltage placed across the device. The CCD was mounted inside an Infrared Laboratories ND-8 3206 liquid nitrogen dewar, a container made specifically to have very good thermal insulation and maintain a high vacuum. The CCD is operated very cold (133 K) to minimize unwanted electrons (the dark current) generated by thermal fluctuations within the silicon lattice, which are independent of any light signal. Dark current effects are reduced significantly at low temperatures. The ultra-high vacuum ($10^{-5}-10^{-7}$) is necessary to draw out vapors that would condense on the CCD when it is cooled, thereby short-circuiting and destroying the device.

The CCD is run by a Leach controller that is itself computer-controlled. The Leach controller is a dual readout controller from Astronomical Research Cameras, Inc. It has several boards which operate and read the CCD. The utility board, based on a Motorola DSP 56001, controls the exposure timing and shutter operation. The timing board, based on a Motorola DSP 56002FC66, generates digital timing signals to control other circuit boards and communicates with the host computer. The video board processes and digitizes the video output from the CCD, and supplies digitally programmable DC bias voltages to the CCD. The clock driver board provides analog voltage levels from +10V to -10V for the clock signals.

To perform characterization experiments, the CCD is illu-

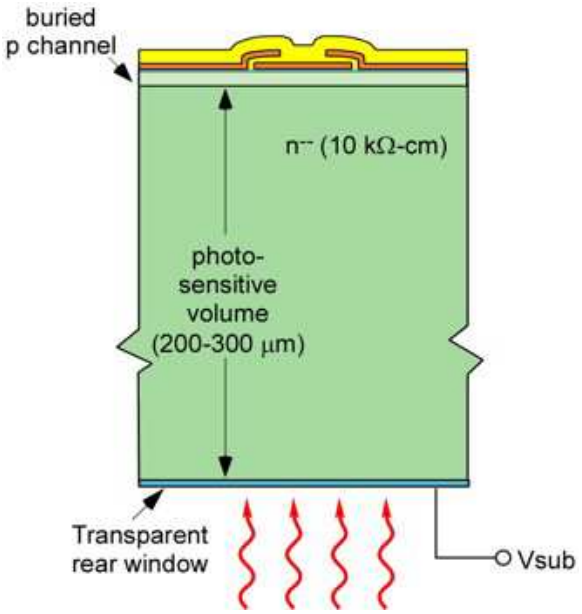

FIG. 3.— Cross-section of the 3-phase LBNL high-resistivity p-channel CCD. Fully depleted operation of these devices is made possible via the application of a substrate bias voltage applied via a backside polysilicon electrode. (courtesy LBNL)

minated by a light source external to the dewar, which forms a point of light on the CCD surface. Light from a high-intensity General Electric bulb passes through a filter before it is focused onto a fiber optic cable bundle. The fiber optic was then fed into a light tight dark box that contained the pinhole projector. The fiber was connected to the pinhole projector that consisted of a horizontal tube with a pinhole and lenses inside it an a focusing optic on its end. A centering assembly holds the fiber optic cable in place inside a brass tube. The light illuminates a 10 μm pinhole, passes through a tube, and is collimated by a tube lens. The collimated light is then focused to about 1 μm on the CCD by a microscope objective with a working distance of 34 mm. The point of light can be moved along both the in the x and y axes relative to the device's planar surface.

Two sets of data were obtained for measuring the variations in sensitivity and spatial fidelity we wish to measure. The first set of data consists of nine pointings equally spaced within a pixel. The second set of data consists of a set of pointings that move consecutively from the interior of the device near the active area edge, outward and across the active area edge into the inactive area that forms a frame around the device and contains circuitry. The data taking procedure proceeded in the following steps. First, by taking consecutive images the point of light was centered on a single pixel. For the first set of images the spot was moved from the center of one pixel across three whole pixels to the center of the fifth pixel. Three images are taken on each pass of a pixel with the points of light spaced evenly across it. Then the procedure is repeated for the upper and lower parts of the pixels, allowing nine samples across three pixels. Another pass is taken across the top of another set of pixels below the first for a total of fifty two pictures for the first set of images. The second set of images starts in the center of one pixel and scans across 61 pixels to the edge of the device with three steps per pixel similar to the first method. However, this time only one pass is taken across all of the pixels.

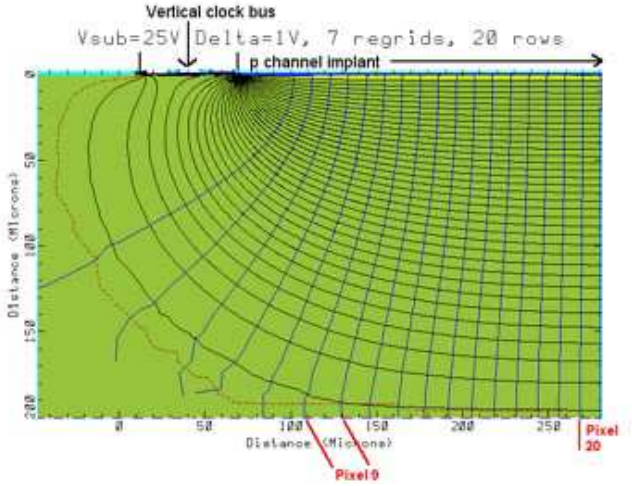

FIG. 4.— TSUPREME simulation of electric fi elds inside the device for low voltage conditions. This simulation suggest that at low voltage conditions additional charge spreading may occur near the device edges. (courtesy LBNL)

3. DATA REDUCTION AND ANALYSIS

The images were processed using a custom made IDL (Interactive Data Language) program. the preliminary data reduction proceeded in three steps. First, the images were converted from FITS files into two-dimensional arrays. Second, the median value was taken for the overscan region associated with the side of the device where the spot was located. This value was subtracted from every pixel on its respective side. Third, a region is selected around the point of light. This region is used in the analysis steps to simplify the computing process. Two sets of images were analyzed in order to measure intrapixel sensitivity variation and spatial distortions, and spatial distortions near the device edge. To understand properly the measurement process we first review the possible sources of error in our data and procedures.

3.1. *Measurement Uncertainties*

There were several possible sources of errors in our experiment and analysis that must be identified and handled. They include the stability of the light source's luminosity, light leaks in the experimental apparatus, exposure time uncertainties due to shuttering, and electronic noise sources in the device and electronics. These systematic errors are independent from measurement values and must be added in quadrature and given as a percentage of the measured values where non-negligible.

3.1.1. *Lamp Stability*

The radiance stability of the lamp depends most on the current supplied and the ambient temperature. The lamp control circuitry is such that it maintains a 0.03% or less drift in the current supplied to the lamp according to calibration data supplied by the manufacturer. The ambient room temperature may in principle also affect the radiance of the lamp. The lamp filament glows due to ohmic heating with Plank's equation governing how temperature effects the change in intensity.

$$I(\lambda, T) = \frac{2hc^2}{\lambda^5} \frac{1}{e^{\frac{hc}{\lambda kT}} - 1}$$

Since the lamp outputs primarily in the visible, we approximate that the peak of the output occurs at around 700nm. A

blackbody curve peaking at 700nm originates from a body at around 4500K. Because the room in which the experiment takes place is temperature controlled to about $\pm$2K then it could only induce $< 0.001\%$ error in the intensity.

3.1.2. *Light Leaks*

The test setup system was built by Masters student Jens Steckert at LBNL during 2006. He monitored light leaks by placing a calibrated photdiode in the dark box. A current of $\approx$ 50 fA was measured in the system with all illumination sources turned off. When the illumination sources were turned on the measured current was > 0.1 nA. Thus, the error contribution of light leaks is negligible.

3.1.3. *Exposure Time Variations*

Calculation of the radiant flux at the CCD surface requires knowledge of the exposure time. In the experimental setup the exposure time is controlled via a Uniblitz shutter, which takes time to open and close. During this time, the positions of the shutter blades are unknown and somewhere between their open and closed positions. During this time an unknown amount of light may pass through the shutter. In order for the error in a flux calculation to be below 1% the amount of light passing during the opening and closing phases must be less than 1% of the total light incident on the CCD during the exposure time. Uniblitz quotes an opening time of 6 ms and a closing time of 5 ms. The total transfer time during one exposure is thus 11ms. Assuming the shutters are fully transparent during the shutter transfer, the exposure time has to be at least 100 time the transfer time:

$$t_{exposure} \geq 100 \times t_{transfer}$$

. The exposure times in our experiment were 3.0 seconds. Thus, the error contribution from this effect were negligible.

3.1.4. *Electronic Noise*

Next the accuracy of the device and electronics must be taken into account. The device introduces error with shot noise, dark current, pixel non-uniformity and read noise. Shot noise is generated by the random arrival times of photons, which is governed by Poissonian statistics and is therefore equal to the square root of the signal. This error is handled by taking data with large signal levels. We desire precision of at least 1%, thus data was taken with signal levels of at least 10,000 digital units (DU). We next consider dark current. Dark current is the noise that is produced thermally within the device rather than by photons interacting with the device. It can provide a major source of noise especially in long exposures. As will be described below, we removed the dark current during data reduction by subtracting any background signal surrounding our spot. Read noise is the random noise introduced by the on-chip amplifier and is unrelated to the signal level or exposure time. We can not eliminate the read noise but we can measure it and take it into consideration in quoting our measurement values. To find the read noise an empty column was selected from an overscan subtracted image and converted into an array. Then the median of the array was calculated and divided from every point in the array. A histogram was made from the array and a gaussian was fitted to it. The standard deviation of the gaussian is the read noise. The calculated read noise was 0.418 DU. For signal levels greater than 10,000 DU per pixel, this represents a negligible error. Noise is also generated in the off-chip electronics including the pre-amplifier, amplifier, and the analog to digital converter when a digital interpretation is made out of an analog charge. These noises are removed via overscan subtraction.

In general the signal to noise ratio is equal to this equation:

$$SNR = \frac{P \times QE \times \Delta t}{\sqrt{(P+B)QE \times \Delta t + D\Delta t + {\sigma_R}^2}}.$$

Here P is the photon flux, QE is the device quantum efficiency, B is any background contribution, D is any dark current contribution, σ_R is the read noise, and Δt is the exposure time. In our case here the background, dark current and read noise contributions are negligible.

3.2. *Background Subtraction and Signal Measurement*

Three methods were used to determine total signal from the light source. The three methods differed in the way that background subtraction for minimizing spurious CCD signals was handled.

The first method was to fit a two dimensional gaussian to the spot. The gaussian uses the following equation to fit the curve to.

$$F(x,y) = A_0 + A_1 e^{\frac{-\frac{x}{a}^2 + \frac{y}{b}^2}{2}}$$

Where A_0 is the constant that represents how high the surrounding region is above zero, A_1 represents the amplitude of the Gaussian, a represents the standard deviation of the spot in the x-direction, and b represents the standard deviation of the spot in the y-direction. To obtain the total spot signal we first removed the background. The value A_0 was subtracted from every pixel in the region. Because this should bring the background pixels to zero, the gaussian was then integrated by adding up the value of all the pixels in the region. The drawbacks of this method are that the Gaussian fit is an approximation to the actual spot signal and that it is assumed that the background value of each pixel is equal.

The second method was called the sky subtraction method. Several rows and columns near the edge of the region were selected and the median of each was found. The median rather than the mean was used so as to reduce the offset caused by cosmic rays. The median values were then averaged. This value was subtracted from every pixel in the region reducing the "sky" around the "star" to a value near zero. Then all the pixels in the region were summed. The primary weakness in this method is that it assumes that the background contribution to each pixel is constant.

The final method was utilized a pointwise relaxation method. An image of the background of the region is generated by holding the region's edge pixels constant and point relaxing the interior of the image. The result is a minimal-area surface stretched between the edge pixels, which are assumed to be background. It is similar to the the minimum area surface a soap film would make between an outer ring. This smoothed surface is used as a mask and subtracted from the original region. Fig. 5 shows the pixel-sampled "soap film" mask determined from the data. Similar to the previous two methods this post masked surface is summed to obtained the total signal of the region. This method has the advantage over the previous two methods that any background gradients from top to bottom or left to right in the region are handled nicely. For the isolated feature that we analyze in this paper, this method is most likely the best approach. In a crowded

field more complex methods from those utilized here may be necessary.

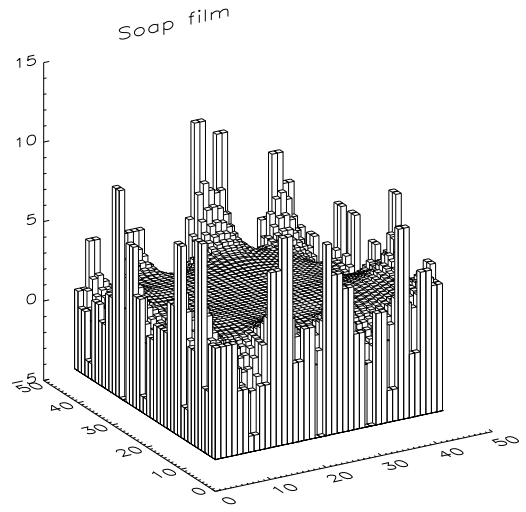

FIG. 5.— Illustration of the soap film background subtraction technique. The raw image is used to generate a background mask by holding the edge pixels of the region constant and point relaxing the interior. The mask is then subtracted from the original images. The surface generated by the point relaxation technique is sampled by the CCD pixel scale in the image shown.

The data obtained from the three methods were all saved in a file from which several graphs were made to visualize and analyze the data. In our final implementation all the three methods agreed to better than 1%.

To perform the analysis of spatial distortions near the device edge a program was also written in IDL very similar to the first. It took the series of images one by one and converted them to arrays. It does the overscan subtraction and creates a region around the spot. Since the point of this data set is to observe the spot's shape near the edge it is important to have accurately fit our two-dimensional Gaussian to the data. However, due to higher pixel values near the edge of the device sometimes the fitting routine would not converge properly. To avoid this problem an identically sized region was selected near the spot in the same orientation. This region could then be subtracted from the first to remove the slightly elevated columns near edge thus allowing the Gaussian fit routine to properly converge. The gaussian fit then could be used to graph the width, in both x and y, of the point as it approached the edge to observe any distortions.

4. RESULTS

The purpose of analyzing the first set of data is to measure any intrapixel and pixel to pixel variations in the CCD. Fig. 6 shows the signal levels of each of the 39 pointings across the five pixels with nine equally spaced pointings for the center three pixels. Fig. 7 shows the centroids calculated from the pointings. The residuals of the intrapixel variations about the

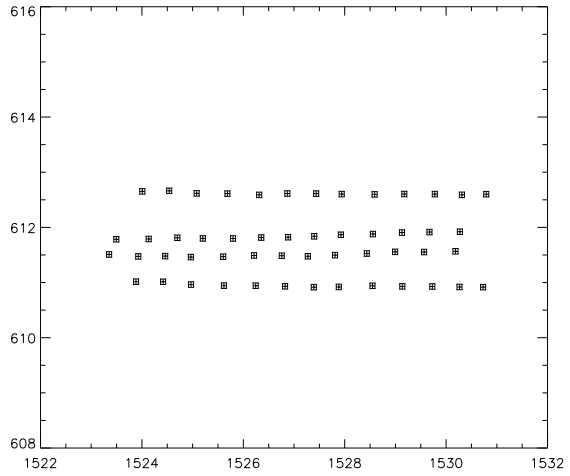

FIG. 7.— Centroid positions measured for the 39 pointings where the central 27 columns are nine by nine pointings within individual pixels.

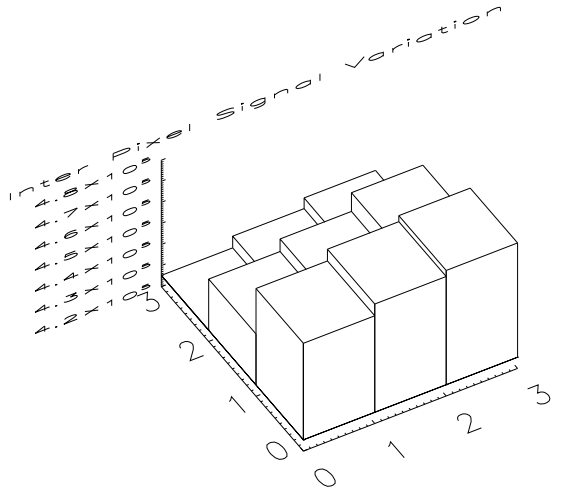

FIG. 6.— Master pixel comprised by the averages of 52 images with nine pointings in each pixel.

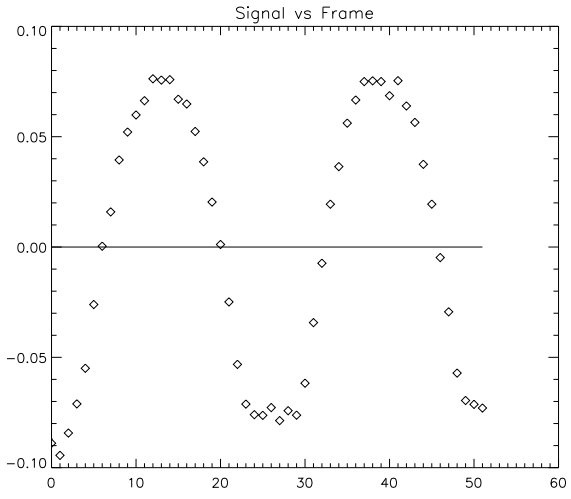

FIG. 8.— Residuals from the mean of the intrapixel signal values presented in Fig. 6. The sensitivity of the device increased systematically as the spot projector moved from left to right across the device. The regular modulation of the signal is caused by the order in which the images were taken as the projector moved from left to right, right to left, and then left to right across the device. Variations are observed at the level of $\pm 10\%$.

mean can also be seen in Fig. 8, where the integrated percent error is graphed versus frame number. The values vary approximately ±10%. We also note a trend of greater sensitivity as the spot is moved from left to right in the data. Because the scans moved across the device from left to right, then right to left, then left to right to form three rows, the residuals show the regular modulation observed in Fig. 8. We also utilize the interior pixels from the edge scan data to investigate intrapixel variations across the centers of about fifty pixels. The residuals of their signals from their average signal are shown in Fig. 9. The values vary approximately ±1.5% and do not show the modulation observed near the device center.

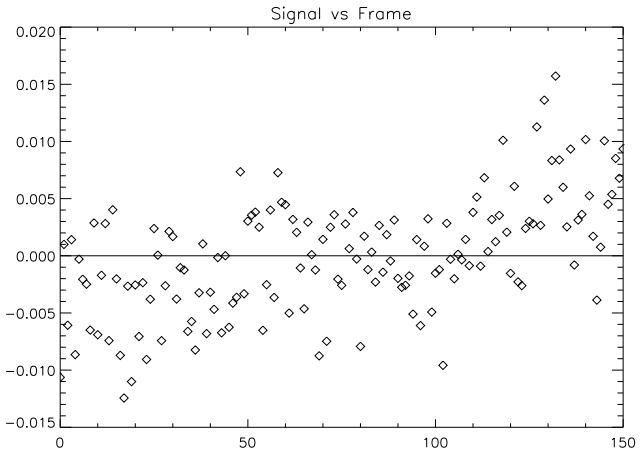

FIG. 9.— Residuals of signal values from the mean obtained across fi fty pixels in a different area of the the device. The variation in these pixels are within ±1.5%.

The second set of data was analyzed to determine and quantify any spatial distortion caused by non-uniform electric fields near the edge of the device as predicted by the TSUPREME simulation. The standard deviations(σ) of the 2-dimensional Gaussian fit values of the spot were plotted for both the x (σ_x) and y (σ_y) axes versus their respective frames. The σ_x plot appeared relatively constant with some slight variations around the edge as seen in Fig. 10. The σ_y plot shows that it was constant most of the way across the device until it reached about 20 pixels from the edge when its size began increasing dramatically until it reached the edge as seen in Fig. 11. The value of σ_y increases at power law rate of $y = x^{1.2}$.

5. CONCLUSIONS

The *Supernova Acceleration Probe* needs its CCDs to have a high degree of accuracy to be able to carry out its mission. The LBNL CCDs, which are planned for SNAP, must have very low intrapixel variations and must have high spatial fidelity across the devices. We have made the first measurement of the sensitivity and spatial variations of these devices at the intrapixel leve. The errors present in the analysis were considered negligible and therefore did not affect the results.

After analyzing this high-resistivity, p-channel CCD it was shown that intrapixel variations varied depending on the region of the device that was measured. At one location the variations were within specifications while at a different location they were not. Previous measurements of these devices have indicated that backside anti-reflection (AR) coating non-uniformities may sometimes be present (Oluseyi et al. 2004). We anticipate this is the cause of the discrepant results. The device examined in this experiment as well as the device that previously showed AR-coating irregularities were backside treated a the Microsystems Laboratory at LBNL, which is setup primarily for research. The device manufacturing is currently being commercialized through DALSA Semiconductor, Inc. It is anticipated that in the commercial environment non-uniformities will be reduced. Nonetheless, this result illustrates the importance for measuring sensitivity at the intrapixel level.

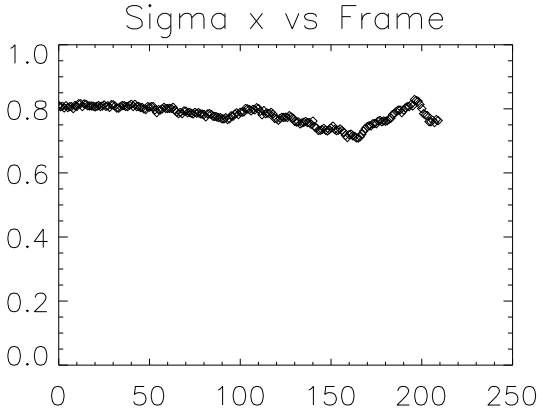

FIG. 10.— Measured values of σ_x versus frame as the spot is scanned across the device edge where frame 210 is the edge of the device.

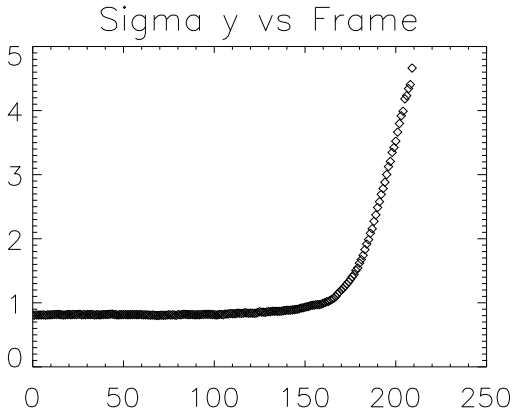

FIG. 11.— Measured values of σ_y versus frame as the spot is scanned across the device edge where frame 210 is the edge of the device.

We have illustrated that spatial distortions do indeed occur at the device edges when low bias voltages are applied due to internal electric field divergence. The result is an effective diffusion in the vertical direction on the device. A substrate voltage of 40V applied to a 300 μm thick device yields the outer 20 pixels of the device unusable for weak lensing science. SNAP envisions using 200 μm thick devices with substrate voltages exceeding 100V (Aldering et al. 2004). These devices will suffer far less effective diffusion from electric field divergence. Analysis of data taken on these devices will be necessary to fully understand this phenomenon.

These initial measurements of SNAP's CCDs will ensure that the necessary steps are taken for accurate data analysis thus increasing our understand of dark energy.

This project was funded by a partnership between the National Science Foundation (NSF AST-0552798), Research Experiences for Undergraduates (REU), and the Department of Defense (DoD) ASSURE (Awards to Stimulate and Support Undergraduate Research Experiences) programs. I also want to thank Pat Malvoso for all his help for all his help in setting up and getting IDL running properly and for his computer expertise throughout the research. Hakeem Oluseyi and Pat Malvoso were supported by the National Science Foundation under Grant No. 0449962. Any opinions, findings, and conclusions or recommendations expressed in this material are those of the authors and do not necessarily reflect the views of the National Science Foundation.

REFERENCES

Aldering, G., et al. 2002, Proc. SPIE, 4835, 146
Aldering, G., et al. 2004, astro.ph, 5232
Bebek, C. J.; Groom, D. E.; Holland, S. E.; Karcher, A.; Kolbe, W. F.; Levi, M. E.; Palaio, N. P.; Turko, B. T.; Uslenghi, M. C.; Wagner, M. T.; Wang, G. 2002, Proc. SPIE, 4669, 161
Dawson, K., Bebek, C., Emes, J., Holland, S., Jelinsky, S., Karcher, A., Kolbe, W., Palaio, N., Roe, N. A., Takasai, K., Wang, G. 2006, IEEE NSS/MIC 9872, 152
Fairfield, J. 2006, IEEE Trans. Nucl. Sci., 53 (6), 3877
Holland, S. E.; Goldhaber, G.; Groom, D. E.; Moses, W. W.; Pennypacker, C. R.; Perlmutter, S.; N. Wang, W.; Stover, R. J.; and Wei, M. 1996, IEDM Technical Digest, 911, 1
Holland, S.E., Wang, N.W., Moses, W. W. 1997, IEEE Trans. Nucl. Sci., 44(3), 443
Holland, S. E., Groom, D. E., Palaio, N. P., Stover, R. J., Wei, M. 2003, IEEE Trans. El. Dev., 50 (3), 225
Hubble, E. 1929, PNAS, 15, 168
Karcher, A.; Bebek, C. J.; Kolbe, W. F.; Maurath, D.; Prasad, V.; Uslenghi, M.; Wagner, M. 2003, IEEE Trans. on El. Dev., 50 (3)
Marshall, C. J., Marshall, P. W., Wacynski, A., Polidan, E., Johnson, S. D., Campbell, A. 2004, Proc. SPIE, 5499, 542
Oluseyi, H. M., Bebek, C. J., Holland, S. E., Levi, M., Karcher, A., Kolbe, W., Roe, N., Uslenghi, M. 2004, Proc. SPIE, 5570, 515
Oluseyi, H. M., Nikzad, S., Blacksberg, J., Hoenk, M. 2005, Proc. SPIE, 5578, 387,
Perlmutter, S., et al. 1999, ApJ, 517, 406
Riess, A. G., et al. 1998, AJ, 116, 1009
Stover, R. J., Wei, M., Lee, Y., Gilmore, D. K., Holland, S. E., Groom, D. E., Moses, W. W., Perlmutter, S., Goldhaber, G., Pennypacker, C. R., Wang, N. W., Palaio, N. 1997, Proc. SPIE, 3019, 183